IEEE Access
Multidisciplinary : Rapid Review : Open Access Journal

Received November 1, 2019, accepted November 10, 2019, date of publication November 12, 2019,
date of current version November 26, 2019.

Digital Object Identifier 10.1109/ACCESS.2019.2953224

Sensitivity Comparison of Open-Circuit Airgap Flux Between Surface-Mounted Permanent Magnet and Spoke-Type Permanent Magnet Machines Considering Manufacturing Tolerances

CHA-SEUNG JUN[1], (Member, IEEE), OHBONG KWON[2], (Member, IEEE), AND BYUNG-IL KWON[3], (Senior Member, IEEE)
[1]Appliance Research and Development Laboratory, LG Electronics Inc., Seoul 08592, South Korea
[2]New York City College of Technology, New York, NY 11201, USA
[3]Department of Electronic Systems Engineering, Hanyang University, Ansan 15588, South Korea

Corresponding author : Byung-Il Kwon (bikwon@hanyang.ac.kr)

This work was supported in part by the BK21PLUS Program through the National Research Foundation of Korea within the Ministry of Education, and in part by the National Research Foundation of Korea (NRF) grant funded by the Korea Government (Ministry of Science) under Grant NRF-2017R1A2B4007697.

ABSTRACT The study compares the sensitivities of open-circuit airgap flux (OCAF) between a surface-mounted permanent magnet (SPM) machine and a spoke-type PM machine based on variations in airgap length including additional airgaps between permanent magnets and rotor core and between segmented stator cores to achieve high quality electric machines. Analytical equations deduced from magnetic equivalent circuits (MECs) are used to directly compare natural-born characteristics of the OCAF of the two machines. First, the MEC of each machine is modeled by considering two additional airgaps between the PMs and rotor core and between the segmented stator cores. Second, the OCAF equation of each machine is derived from the MEC to analyze the effects of the design variables on the OCAF. Subsequently, the partial derivative equation of the OCAF equation with respect to the airgap length is obtained for sensitivity analysis. A comparison of the equations of the two machines indicates that the spoke-type PM machine exhibits inherently higher sensitivity and average value of the OCAF when compared to that of the SPM machine. Finally, the results are validated via a two-dimensional finite element method (FEM) by considering the variations in airgap lengths.

INDEX TERMS Air-gap flux, magnetic equivalent circuit, permanent magnet machine, sensitivity, SPM, Spoke-type.

I. INTRODUCTION

Recently, high efficiency of electric machines corresponds to the most important performance metric to satisfy increased energy regulations and standards in all application fields. To achieve higher efficiency, permanent magnet (PM) machines are widely used instead of induction or DC motors [1]–[5]. Specifically, flux-concentrating structures, such as spoke-type PM machines or V-shaped PM machines, are continuously developed [6]–[12] because they can provide higher open-circuit airgap flux (OCAF) when compared to the conventional PM machines.

However, spoke-type PM machines also exhibit complicated rotor structures that can cause higher performance variation due to the manufacturing tolerances and higher manufacturing cost. It weakens competitiveness by offsetting the advantages of spoke-type PM machines. In severe cases, the competitiveness of the normally designed spoke-type PM machines is lower than that of the optimally designed SPM machine. Hence, SPM machines are widely used for many applications with the exception of high-speed applications that normally adopt SPM machine [13]–[16]. Thus, it is important to control performance variation due to the manufacturing tolerances of spoke-type PM machines.

High-quality electric machines should satisfy lower probability of failure (POF) and higher performance [17], [18]. With respect to lower POF, a few studies investigated how

The associate editor coordinating the review of this manuscript and approving it for publication was Xiaodong Sun.

manufacturing tolerances in SPM machines affect machine performance [19]–[28]. Furthermore, some articles presented a robust design for PM machines for low POF [18], [29]–[31].

However, most of the aforementioned articles used complicated analytical equations or regression equations, which can be reasonable for the special case, obtained via finite element method (FEM) to investigate the effects of uncertainties, such as manufacturing tolerances and variations in material properties, on the cogging torque and torque ripple. The aforementioned methods are not suitable to directly investigate the effects of design variables on the machine performance.

Additionally, there is a paucity of research on the robustness regarding OCAF characteristics although the OCAF is a basic characteristic that determines machine performance. Furthermore, only a few studies compare tolerance sensitivities of the OCAF between different types of machines such as spoke-type PM machines and SPM machines.

The study compares tolerance sensitivities and magnitudes of the OCAF between SPM and spoke-type PM machines with manufacturing tolerances to compare their relatively inherent tolerance sensitivity and the magnitude of the OCAF and to analytically investigate the effect of design variables such as airgap length, PM thickness, and PM width.

First, the magnetic equivalent circuit (MEC) of each machine is modeled by considering the additional airgap between PMs and rotor back yoke and between segmented stator cores. Subsequently, the OCAF equation of each machine is deduced from the MEC to analyze the effects of design variables on the OCAF. Subsequently, the partial differential OCAF equation with respect to the variation in design variables of each machine is deduced from the OCAF equation for the sensitivity analysis.

Next, tolerance sensitivities of the two machines are directly compared using the equations to verify inherently different OCAF characteristics with an example study.

Finally, the analysis results are validated by an example study performed via a two-dimensional (2D) finite element method (FEM) and Monte-Carlo simulation (MCS) to visualize distributions of the OCAFs with variations in design variables.

II. SENSITIVITY ANALYSIS USING MEC EQUATIONS

The sensitivity analysis is performed by using the MEC method considering the manufacturing tolerances of the airgap variations including additional airgap between PM and rotor core since the MEC method provides a better understanding or some restricted general result with respect to design variables irrespective of machine specifications such as machine size and materials.

A. IMPORTANCE OF TOLERANCE SENSITIVITY

It is widely known in quality control engineering that performance variations increase in a system with complex structures or a large number of components. Thus, the variation increases even if the mean value of performance improves, which can result in the absence of a statistical difference in performance from the existing one as shown in Fig. 1 (a). Conversely, Fig. 1 (b) shows improved mean and variation in the performance. The situation in Fig. 1 (a) can also occur while developing electric machines, and thus machine engineers should carefully consider tolerance sensitivity from the design stage.

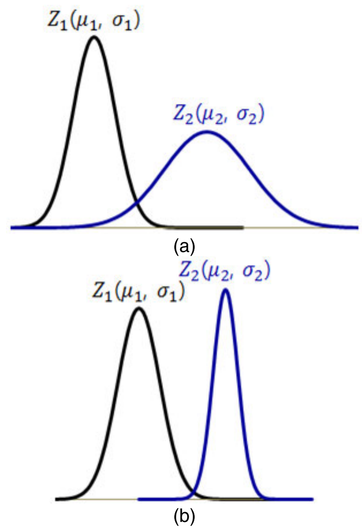

FIGURE 1. Effect of tolerance sensitivity (standard deviation or variation) on performance before and after improvement (a) Statistically no difference, (b) Difference.

B. MODELING FOR MEC

Generally, the OCAF Φ_g and its variation significantly affect machine performance such as the back-electromotive force (Back-EMF), torque characteristics, and control strategy in the flux weakening region. Thus, the tolerance sensitivity of the OCAF should be examined with respect to design parameters in detail while analyzing and designing PM machines.

In the study, the OCAF of a SPM and a spoke-type PM machines are compared with respect to mean value and its variation caused by the manufacturing tolerances. It specifically focuses on the effect of the airgap lengths variation because the most effective factor of the manufacturing tolerances that affects performance variation or tolerance sensitivity of the electric machines corresponds to the airgap length including additional airgaps generated while producing and assembling each part of the machine.

The MEC method and its analytical equation are used to compare the OCAF characteristics of the two machines in the general case and not in the special one. This accounts for additional airgaps described as A and B in Fig. 2. The additional airgap A occurs between segments of the stator core if a segmented core is used to increase the slot fill factor. The other additional airgap B occurs between PMs and rotor core while assembling them.

The stator is composed of a fractional-slot concentrated winding with nine slots, and there are six poles in the rotor. For the MEC analysis, as shown in Fig. 3, the slotted stator core in Fig. 2 is replaced with a ring-type slotless core and

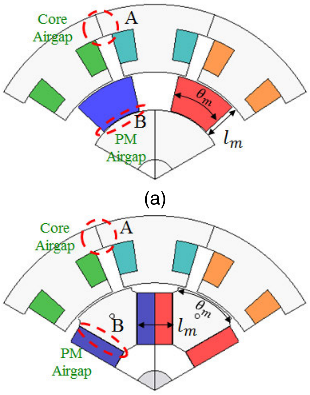

FIGURE 2. Physical analysis models (a) SPM, (b) Spoke-type.

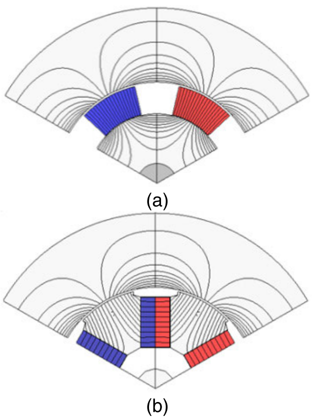

FIGURE 3. MEC models with ring-type stator model and flux lines (a) SPM, (b) Spoke-type.

its effect on the airgap flux is mathematically expressed by the carter coefficient, k_C, in MEC to simplify the analytical models.

TABLE 1 shows the common specifications of the two analysis models.

TABLE 1. Specifications of the analysis models.

Item	Unit	Value
Slot / Pole	-	9 / 6
Winding	-	FSCW
Serial turns per phase	-	480
Stator outside radius	mm	53
Stator inside radius	mm	30.6
Rotor outside radius	mm	30.0
Stack length	mm	35
Core material	mm	50JN1300
Magnet material	-	Ferrite (Br 0.42 T)
Magnet thickness	mm	9.0
Rated torque	N.m	0.5
Rated speed	rpm	2850
DC link voltage	V	310
Rated / max current	A	1.0 / 3.0

C. MEC ANALYSIS EQUATIONS

The basic MECs of the SPM and Spoke-type machines are comprehensively described in [32]. In the study, the effects of the additional airgaps A and B in the two machines in Fig. 2 are included in the MECs.

Figure 4 shows the equivalent linear models and dimension variables of the SPM machine and Spoke-type PM machine corresponding to Fig. 1, respectively. As shown in the figure, the additional airgaps A and B in Fig. 1 are expressed as l_{cg} and l_{mg}, respectively.

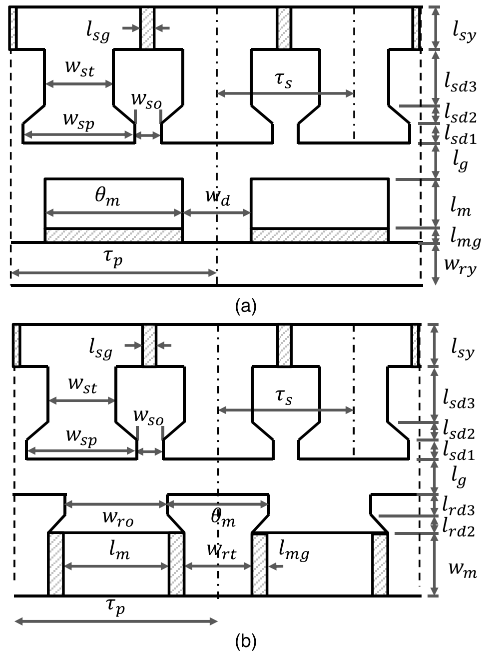

FIGURE 4. Equivalent linear models with variables (a) SPM and (b) Spoke-type.

Figure 5 shows the corresponding full MECs with the ring-type stator core of the two machines in which two additional airgaps are included. Subsequently, the full MECs are simplified via equivalent circuit transformations as shown in Fig. 6.

TABLE 2 describes magnetic reluctance components and flux components used in Fig. 5 and Fig. 6.

TABLE 2. Magnetic reluctance and flux of the analysis model.

Item	Unit
R_{sc}	Stator core
R_g	Airgap
R_{lm}	PM mutual-leakage
R_m	PM
R_{ls}	PM self-leakage
R_{mg}	PM additional airgap
R_{ry}	Rotor core
R_{m2}	$R_m + R_{mg}$
Φ_g	OCAF
Φ_{ls}	Self-leakage flux of PM
Φ_{lm}	Mutual-leakage flux of PM
Φ_r	Residual flux of PM
Φ_{r2}	Residual flux of PM including effect of R_{mg}
R_{sc}	Stator core

TABLE 3. **Comparison of the MEC equations between SPM and spoke-type PM machines.**

Equation of SPM machine		Equation of Spoke-type PM machine	
$\Phi_{g,SPM} = \dfrac{K_l A_m B_r}{1 + \dfrac{\mu_r l_{mg}}{l_m} + \dfrac{\mu_r K_r K_a l_{ge}}{l_m}}$	(1)	$\Phi_{g,Spk} = \dfrac{2K_l A_m B_r}{1 + \dfrac{\mu_r l_{mg}}{l_m} + 4\dfrac{\mu_r K_r K_a l_{ge}}{l_m}}$	(2)
$B_{g,SPM} = \dfrac{K_l K_a B_r}{1 + \dfrac{\mu_r l_{mg}}{l_m} + \dfrac{\mu_r K_r K_a l_{ge}}{l_m}}$	(3)	$B_{g,Spk} = \dfrac{2K_l K_a B_r}{1 + \dfrac{\mu_r l_{mg}}{l_m} + 4\dfrac{\mu_r K_r K_a l_{ge}}{l_m}}$	(4)
$S_{g,SPM} = \dfrac{\partial B_g}{\partial l_g} = \dfrac{-K_l \mu_r K_r K_a^2 B_r}{l_m \left[1 + \dfrac{\mu_r l_{mg}}{l_m} + \dfrac{\mu_r K_r K_a l_{ge}}{l_m}\right]^2}$	(5)	$S_{g,spk} = \dfrac{\partial B_g}{\partial l_g} = \dfrac{-8K_l \mu_r K_r K_a^2 B_r}{l_m \left[1 + \dfrac{\mu_r l_{mg}}{l_m} + 4\dfrac{\mu_r K_r K_a l_{ge}}{l_m}\right]^2}$	(6)

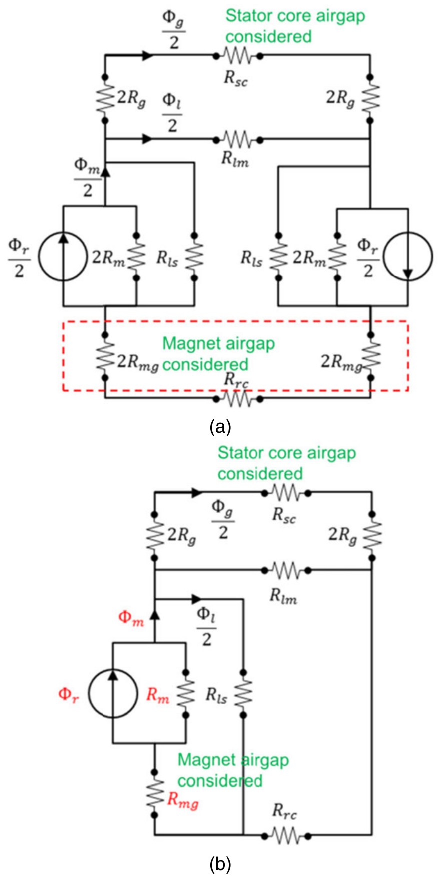

FIGURE 5. **Full MEC models with ring-type stator model (a) SPM, (b) Spoke-type.**

TABLE 2 describes magnetic reluctance components and flux components used in Fig. 4 and Fig. 5.

By solving the MECs with respect to the OCAF, the OCAF equations of the two machines are deduced as (1) to (4) shown in TABLE 3 where A_m denotes the cross-sectional area of a PM, A_g denotes the cross-sectional area of the airgap per pole, B_r denotes the residual flux density of PM, μ_r denotes the relative permeability of PM, l_m denotes the thickness of PM,

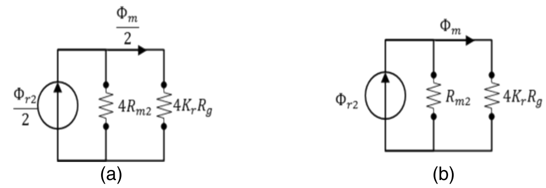

FIGURE 6. **Simplified MEC models with ring-type stator model (a) SPM, (b) Spoke-type.**

l_{mg} denotes the additional airgap between PM and rotor core, l_{ge} denotes the effective airgap length calculated by $K_c l_g$ by considering the Carter coefficient K_c, K_l denotes the leakage coefficient defined by Φ_g/Φ_m, K_r denotes the reluctance coefficient to consider magnetic reluctance of stator core, K_c denotes the Carter coefficient, and K_a denotes the area coefficient defined by A_m/A_g.

In the study, we focus on and examine inherently different characteristics of the airgap magnetic flux density of the two machines due to manufacturing tolerances, especially, variations in the airgap lengths which have a great influence on the electrical machine characteristics.

To focus on the sensitivities of the two machines based on the variations in the airgap lengths, l_g, the sensitivity of each machine can be performed by partially differentiating (3) and (4) with respect to l_g assuming all variables are independent of airgap length. We obtain the sensitivity S_g of each machine as shown in (5) and (6), respectively.

D. ANALYTICAL STUDY USING MEC EQUATIONS

The main purpose of the study is to relatively compare the OCAF characteristics between the spoke machine and SPM machine. Therefore, we make and use indexes for comparing the characteristics.

First, it is necessary to express the airgap length and PM thickness as a variable for normalization. Hence, we use the well-known permeance coefficient, K_{pc}, defined as (7) where K_t denotes the thickness factor defined by l_m/l_{ge}, K_{ac} denotes the additional concentration coefficient to consider the magnetic concentration structure based on machine type, and $K_\emptyset$ denotes the magnetic concentration coefficient.

$$K_{pc} = \frac{-B_m}{\mu_0 H_m} = \frac{A_g l_m}{K_{ac} A_m l_{ge}} = \frac{K_t}{K_\emptyset} \tag{7}$$

$$\text{where } K_{\mathbf{ac}} = 1(SPM) or 2(Spoke-type) \tag{8}$$

The concentration coefficient of the spoke-type PM machine, $K_{\emptyset,Spk}$, is twice that of the SPM machine, $K_{\emptyset,SPM}$, in case of same machine size with the exception of rotor type, i.e., $K_{\emptyset,Spk} = 2K_{\emptyset,SPM}$, and its permeance coefficient is half that of the SPM machine as follows:

$$K_{pc} = K_{pc,SPM} = 0.5K_{pc,Spk} \tag{9}$$

$$K_\emptyset = K_{\emptyset,SPM} = 2K_{\emptyset,Spk} \tag{10}$$

The permeance coefficient determines the operating point on the B–H curve of the PM and permeance coefficients of the two machines are shown in Fig. 7. Spoke-type PM machines should be more carefully designed because they are more easily demagnetized than SPM machines due to the lower permeance coefficient.

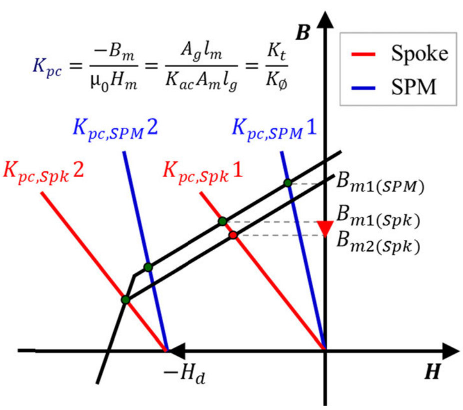

FIGURE 7. Permeance coefficient and operating points based on machine type.

Second, we investigate the term of the additional airgap length l_{mg}. Decreases in l_{mg} improves machine performance and its magnitude depends on machine manufacturing process capability and assembly method. The additional airgap length is typically less than 0.1 mm and PM thickness is more than 2 mm based on demagnetization, productivity, and manufacturing cost, and thus the term of the additional airgap length, $\mu_r l_{mg}/l_m$, is less than 0.2 mm and is expressed by (11) to simplify the equations in TABLE 3.

$$1.0 \leq K_{mg} = 1 + \frac{\mu_r l_{mg}}{l_m} \leq 1.1 \tag{11}$$

Finally, we substitute (7) and (11) into (3) to (6) to obtain (12) to (15) in TABLE 4.

Henceforth, we relatively compare the airgap magnetic flux densities and sensitivities of the SPM machine and spoke machine by assuming same machine dimension, i.e., magnet size, airgap length, etc.

To relatively compare airgap flux density and sensitivity between SPM machine and spoke-type PM machine with respect to the permeance coefficient, we define three relative comparison indexes using equations (12) to (15):

- The ratio of the airgap flux density of the spoke-type PM machine to SPM machine, R_B, is defined by $B_{g,Spk}/B_{g,SPM}$ and is calculated as follows:

$$R_{\mathrm{B}} \equiv \frac{B_{g,Spk}}{B_{g,SPM}} = \frac{2(K_{pc}K_{mg} + \mu_r K_r)}{K_{pc}K_{mg} + 4\mu_r K_r} \tag{16}$$

The index is used to determine the permeance coefficient $K_{pc}(R_{\mathrm{B}})$ that indicates the value that $B_{g,Spk}$ is greater than or equal to $B_{g,SPM}$ based on the permeance coefficient as follows:

$$R_B \geq 1 \rightarrow K_{pc}(R_B) \geq \frac{2\mu_r K_r}{K_{mg}} \tag{17}$$

As shown, $K_{pc}(R_B)$ is only the function of μ_r, K_r, and $K_{mg}(l_{mg}, l_m)$.

- The ratio of the airgap flux density of the spoke-type PM machine to SPM machine, R_{S}, is defined by $S_{g,Spk}/S_{g,SPM}$ and is calculated as follows:

$$R_S \equiv \frac{S_{g,Spk}}{S_{g,SPM}} = \frac{8\left(K_{pc}K_{mg} + \mu_r K_r\right)^2}{\left(K_{pc}K_{mg} + 4\mu_r K_r\right)^2} \tag{18}$$

The index is used to determine the permeance coefficient $K_{pc}(R_{\mathrm{S}})$, which indicates that $S_{g,Spk}$ is greater than or equal to $S_{g,SPM}$ based on the permeance coefficient as follows:

$$R_S \geq 1 \rightarrow K_{pc}(S_B) \geq \frac{0.641\mu_r K_r}{K_{mg}} \tag{19}$$

TABLE 4. Comparison of MEC equations between SPM and spoke-type PM machines.

Equation of SPM machine		Equation of Spoke-type PM machine	
$B_{g,SPM} = \dfrac{K_l K_{\emptyset,spm} B_r}{K_{mg} + \dfrac{\mu_r K_r}{K_{pc,spm}}}$	(12)	$B_{g,Spk} = \dfrac{K_l K_{\emptyset,spk} B_r}{K_{mg} + 2\dfrac{\mu_r K_r}{K_{pc,spk}}}$	(13)
$S_{g,SPM} = \dfrac{-\mu_r K_r K_l K_{\emptyset,spm}^2 B_r}{l_m \left[K_{mg} + \dfrac{\mu_r K_r}{K_{pc,spm}}\right]^2}$	(14)	$S_{g,Spk} = \dfrac{-2\mu_r K_r K_l K_{\emptyset,spk}^2 B_r}{l_m \left[K_{mg} + 2\dfrac{\mu_r K_r}{K_{pc,spm}}\right]^2}$	(15)

It is observed that $K_{pc}(R_B)$ is only the function of μ_r, K_r, and $K_{mg}(l_{mg}, l_m)$.

- The ratio of the sensitivity per airgap flux density of the spoke-type PM machine to that of the SPM machine, R_{SB}, is defined by R_S/R_B or $R_{SB,Spk}/R_{SB,SPM}$ as follows:

$$R_{SB} \equiv \frac{R_S}{R_B} = \frac{S_{g,Spk}}{S_{g,SPM}} \cdot \frac{B_{g,SPM}}{B_{g,Spk}} = \frac{S_{g,Spk}}{B_{g,Spk}} \Big/ \frac{S_{g,SPM}}{B_{g,SPM}} = \frac{R_{SB,Spk}}{R_{SB,SPM}} = \frac{4\left(K_{pc}K_{mg} + \mu_r K_r\right)}{K_{pc}K_{mg} + 4\mu_r K_r} \tag{20}$$

The index is used to determine the permeance coefficient $K_{pc}(R_{SB})$ that indicates the value that $R_{SB,Spk}$ is greater than or equal to $R_{SB,SPM}$ based on the permeance coefficient as follows:

$$R_{SB} \geq 1 \rightarrow K_{pc}(S_{SB}) \geq 0 \tag{21}$$

As shown, $K_{pc}(R_{SB})$ is greater than or equal to zero, which implies that the ratio of the sensitivity per airgap flux density of the spoke-type PM machine, $R_{SB,Spk}$, is always higher or equal to $R_{SB,Spk}$ of the SPM.

By using the deduced equations, we specifically analyze the relative characteristics based on the permeance coefficient when the machine constants in TABLE 5, in which K_l, K_r, and K_c are referred to [20], vary between minimum and maximum of the ranges.

TABLE 5. Ranges of K_l, K_r, K_c, K_a, l_{mg}.

Unit
$0.9 \leq K_l \leq 1.0$
$1.0 \leq K_r \leq 1.2$
$1.0 \leq K_c \leq 1.1$
$0.9 \leq K_a \leq 1.2$
$0.0 \leq l_{mg} \leq 0.1$
$1.0 \leq K_{mg} \leq 1.1$
$1.0 \leq \mu_r \leq 1.05$

First, we examine general trends. Figure 8 shows the comparison results of B_g, S_g, R_B, R_S, and R_{SB} between the SPM machine and spoke-type PM machine. In the figure, the response values are divided by the residual flux density of the PM, B_r, to normalize characteristics irrespective of the PM material.

As shown in Fig. 8, all responses, i.e., B_g, S_g, R_B, R_S, and R_{SB} of the spoke-type PM machine exceed those of the SPM machine,.

Furthermore, it is observed that the variations in the airgap flux densities and sensitivities of the spoke machine exceed those of the SPM machine at the same permeance coefficient, which also implies that the magnetic characteristics related to the airgap flux density of the spoke-type PM machines are more sensitive than that of the SPM machines.

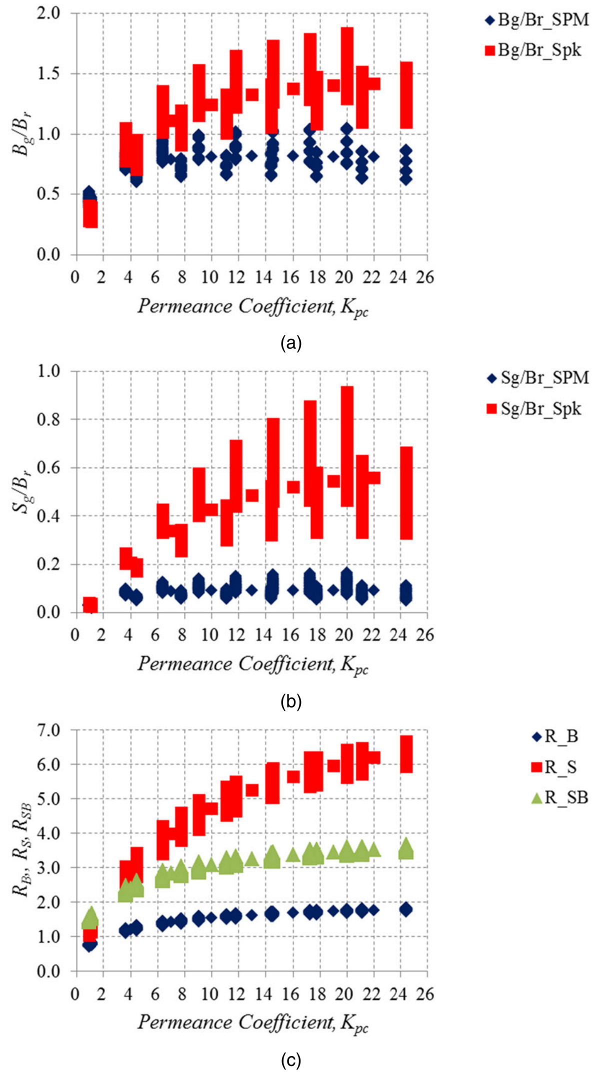

FIGURE 8. Comparison of magnetic characteristics between SPM and spoke-type PM machines whendesign constants in Table 4 varybetween minimum and maximum ofeach range (a) airgap flux density, (b) sensitivity (c) R_B, R_S, an R_{SB}.

Second, we compare and investigate the equations, i.e., (17), (19), and (21) more quantitatively.

Most PM machines should be practically designed to satisfy $4 \leq K_{pc} \leq 6$ [20] to consider demagnetization of PM and manufacturing cost among others, and the following conclusions are obtained:

- Equation (17) indicates that the airgap magnetic flux density of the spoke-type PM machine exceeds that of the SPM machine from the point $2\mu_r K_r/K_{mg}$. The range of the permeance coefficient, K_{pc} (R_B), is $1.82 \leq K_{pc}$ (R_B) ≤ 2.52 in which its maximum value is 2.52 and less than 4. Therefore, it is considered that the airgap magnetic flux density of the spoke-type PM machine exceeds that of the SPM machine in the actual design.
- Equation (19) indicates that the sensitivity of the spoke-type PM machine exceeds that of the SPM machine from the point $0.641\mu_r K_r/K_{mg}$. The range of the

permeance coefficient, $K_{pc}(R_S)$, is $0.58 \leq K_{pc}(R_S) \leq 0.81$ in which its maximum value is 0.81 and less than 4. Therefore, the sensitivity of the spoke-type PM machine exceeds that of the SPM machine in the actual design.
- Equation (21) shows that the sensitivity per airgap flux density of the spoke-type PM machine exceeds that of the SPM machine from point 0. Spoke-type PM machines are always more sensitive than SPM machine in case of the same flux density irrespective of the permeance coefficient.

Third, we compare the characteristics for specific conditions, i.e., $K_l = K_r = K_a = K_c = \mu_r = 1$, $l_{mg} = 0$ mm. Figure 8 and Fig. 9 show magnetic characteristics comparison between the SPM and spoke-type PM machines based on the ratio of the PM length to the airgap length, K_t, at $l_m = 1.0$ mm and at $l_g = 0.5$ mm, respectively.

From Fig. 9, we observe the following:
- As shown in Fig. 9(a), the airgap flux density of the spoke-type PM machine exceeds that of the SPM machine when K_t increases (airgap length decreases).
- As shown in Fig. 9(b), the sensitivity of the spoke machine also exceeds that of the SPM machine when K_t increases (the airgap length decreases), which implies that the spoke-type PM machine is inherently more sensitive to the variation in airgap length than that of the SPM machine due to its magnetic concentration structure.

From Fig. 10, we observe the following:
- As shown in Fig. 10(a), the airgap flux density of the spoke-type PM machine exceeds that of the SPM machine when K_t increases (PM thickness increases) and Fig. 10(a) is identical to Fig. 9(a).

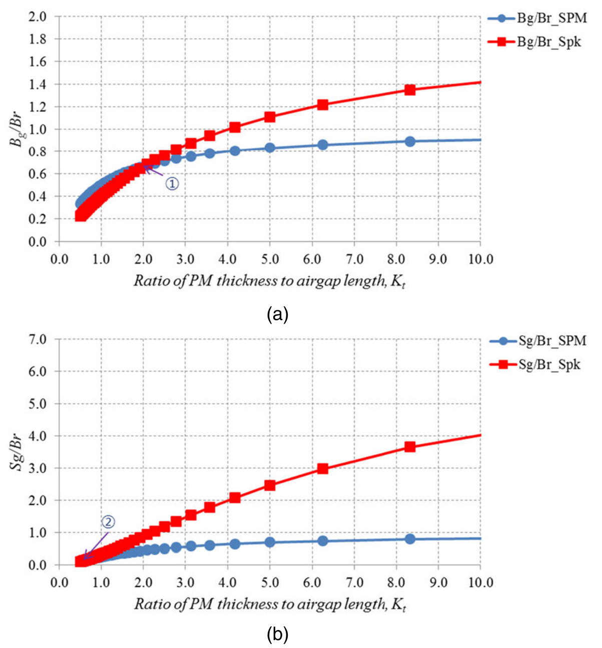

FIGURE 9. **Magnetic characteristics comparisons between SPM and spoke-type PM machines based on the airgap lengthat $K_l = K_r = K_\phi = K_c = \mu_r = 1$, $l_{mg} = 0$ mm, and $l_m = 1.0$ mm (a) B_g/B_r, (b) S_g/B_r.**

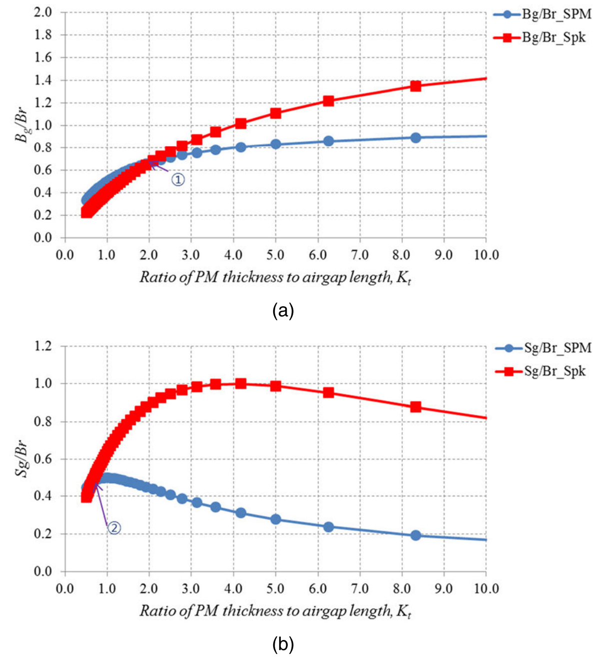

FIGURE 10. **Magnetic characteristics comparisons between SPM and spoke-type PM machines based on thePM length at $K_l = K_r = K_\phi = K_c = \mu_r = 1$, $l_{mg} = 0.0$ mm, and $l_g = 0.5$ mm (a) B_g/B_r, (b) S_g/B_r.**

- As shown in Fig. 10(a), the sensitivity of the spoke machine exceeds that of the SPM machine irrespective of the PM thickness with the exception that it is very small, which implies that the spoke-type PM machine is inherently more sensitive to the variation in the airgap length than that of the SPM machine. In contrast to the sensitivity characteristic with respect to the airgap length, the sensitivity increases initially when PM thickness increases although it decreases when PM thickness exceeds a certain length irrespective of machine type. Therefore, it is necessary to increase PM thickness to the maximum possible extent to increase airgap flux density and also decrease sensitivity. However, the method of increasing PM thickness can lead to an increase in the material cost.

Figure 11 compares the three comparison indexes between the SPM machine and spoke-type PM machine when the machine constants vary between minimum values and maximum values (indicated by "org" in parentheses), as shown in Fig. 8(c), and when they correspond to specific conditions, i.e., $K_l = K_r = K_a = K_c = \mu_r = 1$, $l_{mg} = 0$ mm (indicated by "con" in parentheses).

As shown in the figure, the overall trend is consistent with the previous results; $K_{pc}(R_B)$, point ①, $K_{pc}(R_S)$, point ②, and $K_{pc}(R_{SB})$, point ③, correspond to 2.0, 0.641, and 0, respectively, and the values are equal to those calculated by (16), (18), and (20).

III. VERIFICATION USING 2D-FEM

To verify the MEC results, 2D-FEM is performed based on the variations in the airgap length and PM thickness.

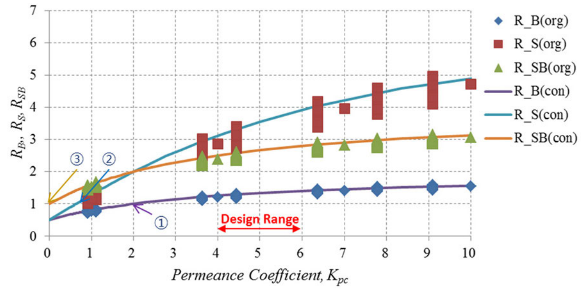

FIGURE 11. R_B, R_S, and R_{SB} based on the permeance coefficient at $K_l = K_r = K_\phi = K_c = \mu_r = 1$, $l_{mg} = 0$ mm.

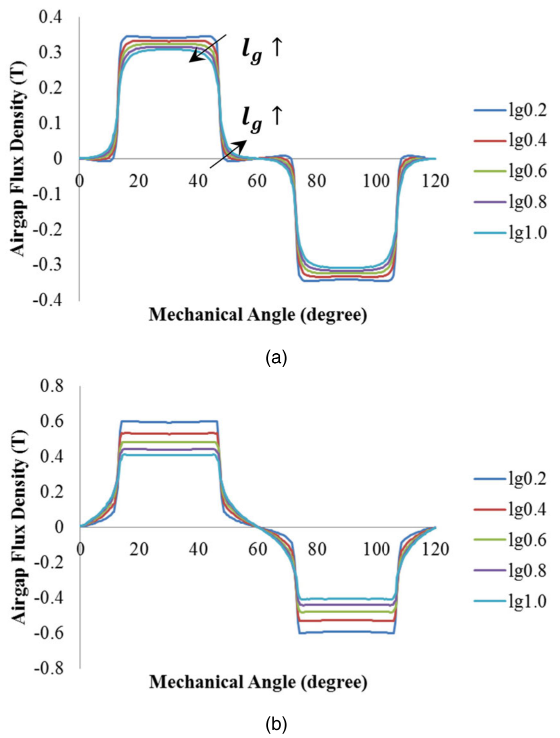

FIGURE 12. Comparison of the airgap flux densiyand sensitivity analyzed by the FEM and MEC based on the airgap lengths (a) Distributions of the airgap flux density of the SPM, (b) Distributions of the airgap flux density of the spoke-type.

A. AIRGAP FLUX DENSITY IN SLOTLESS STATOR

Figures 12(a) and 12(b) show the airgap flux density distributions of the two machines based on the airgap lengths of the ring-type stator models with a PM thickness of 9.0 mm as shown in Fig. 3, respectively. As shown in the figure, the values and variations in the airgap flux densities of the spoke-type PM machine exceed those of the SPM machines.

Figure 13 shows the normalized airgap flux densities, sensitivities, and three relative comparison indexes of the two machines based on airgap lengths, and the values obtained from the FEM are also compared to those of MEC analysis, in which the labeled "MEC1" denotes the specific result that is calculated when $K_l = 0.9, K_r = 1.2, K_a = 0.84$, $K_c = 1.0, \mu_r = 1.05, K_{mg} = 1.0$ in the MEC for comparison with corresponding FEM results.

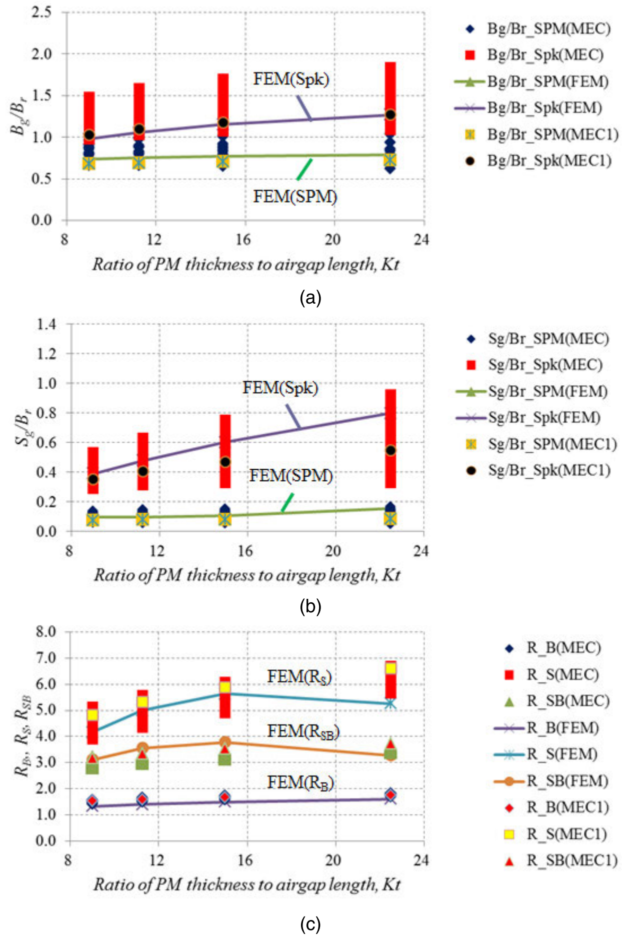

FIGURE 13. Comparisos of the normalized airgap flux densities, sensitivities, and magnetic indexes, analyzed by FEM and MEC, between SPM and spoke-type PM machines based on the ratio of the PM thickness to the airgap length, $K_t l_m$ = 9.0 mm() a) normalized airgap flux density, b) normalized sensitivit, and (c) relative comparison indexes, i.e., R_B, R_S, and R_{SB}.

Figure 13(a) compares the normalized airgap flux density between the SPM and spoke-type PM machines. The trends of the FEM results of the two machines are consistent with the MEC analysis results as shown in Fig. 8(a). In terms of analysis errors between MEC and FEM, it is observed that the FEM values of the two machines are included in the analysis ranges obtained by MEC. The magnitudes of the errors between FEM and MEC1 range from 7.7% to 8.8% for the SPM machine and 0.1% to 5.1% for the spoke-type PM, and the errors appear as reasonable.

Figure 13(b) compares the normalized sensitivities between the SPM and spoke-type PM machines. The trends of the FEM results of the two machines are consistent with the MEC analysis results shown in Fig. 8(b). In terms of analysis errors between FEM and MEC1, it is observed that the FEM results are included in the analysis ranges obtained by MEC.

However, the magnitudes of the sensitivity errors between FEM and MEC1 range from 20.3% to 45.3% for the SPM machine and 9.5% to 31.3% for the spoke-type PM machine although the errors of the airgap flux densi-

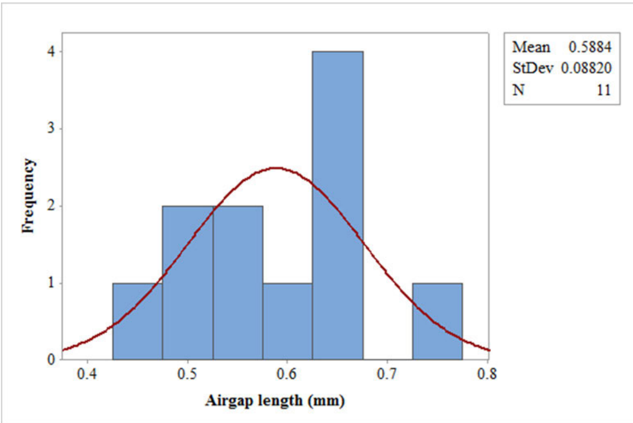

FIGURE 14. **Histogram of the airgap lengths following the normal distribution, i.e., $l_g \sim N(0.5884, 0.0882)$.**

ties of the two machines are less than 10%. Specifically, the error increases as the airgap length decreases or K_t increases, thereby implying that some magnetic constants, e.g., K_l and K_a, are a function of the airgap length and should be treated as a variable as opposed to a constant. Sensitivity is obtained by differentiation, and thus it can significantly vary even with a small difference and it is not easy to fit correctly. Hence, the accurate matching of the constants based on magnetic theory constitutes another issue of the MEC theory and requires significant data analysis and experience. The main objective of the study involves verifying the relative sensitivity of the airgap flux density between SPM and spoke-type PM machines, and thus an accurate modeling study is not performed.

Figure 13(c) compares the three comparison indexes, i.e., R_B, R_S, and R_{SB}, between the SPM and spoke-type PM machines. The trends of the FEM results of the two machines are consistent with the MEC analysis results shown in Fig. 8(c), and all responses exceed one.

Hence, the spoke-type PM machine exhibits higher airgap flux density and sensitivity than those of the SPM machine. In terms of analysis errors between FEM and MEC1, it is observed that the FEM results are included in the analysis ranges obtained by MEC and magnitudes of the errors between FEM and MEC1 range from 9.8% to 13.9% for R_B, 1.1% to 18.1% for R_S and 2.3% to 11.5% for R_{SB}, respectively.

B. PERFORMANCE SENSITIVITY IN SLOTTED STATOR

Using the 2D-FEM with rotor rotating condition for the characteristics comparison between the two machines, we examine more actual cases via the Monte-Carlo simulation [7] by considering the slotted stator in Fig. 2 and variation in the airgap length due to the manufacturing tolerance. The variation in the airgap length follows the normal distribution, i.e., $l_g \sim N(0.5884, 0.0882)$ and are examined with 11 cases as shown in Fig. 14.

Figure 15 compares the OCAF and its standard deviation, which is proportional to the sensitivity between the two

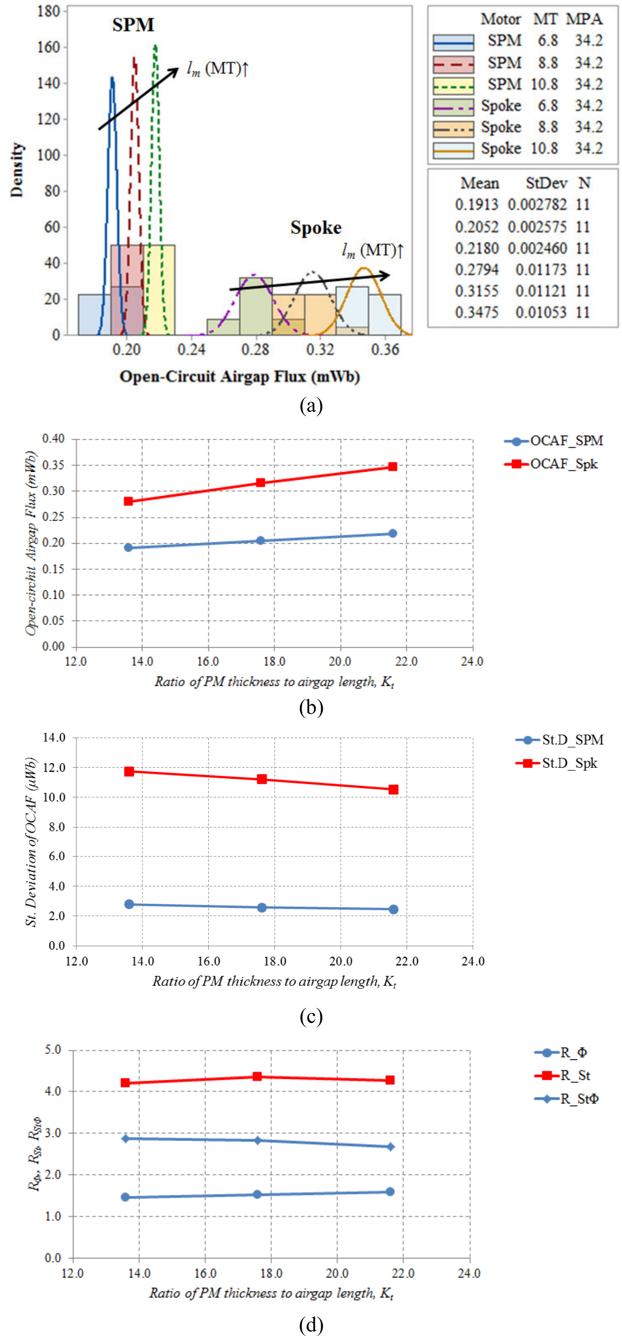

FIGURE 15. **Comparison of open-circuit airgap fluxes (OCAFs)analyzed by FEM between SPM and spoke-type PM machines inslotted stator based on the PM thicknessand variations in airgap length due to manufacturing tolerance (a)Probability distributions, (b) Mean values, (c) Standard deviations, and (d) Relative comparison indexes.**

machines based on the PM thickness (MT) and the same rotor magnetic pole angle (MPA). As shown in the figure, means and standard deviations of the spoke-type PM machine exceed those of the SPM machine. Additionally, increases in PM thickness increases the OCAF mean value although the standard deviation decreases irrespective of machine type.

Figure 16 compares the average torque and its standard deviation between the two machines based on the

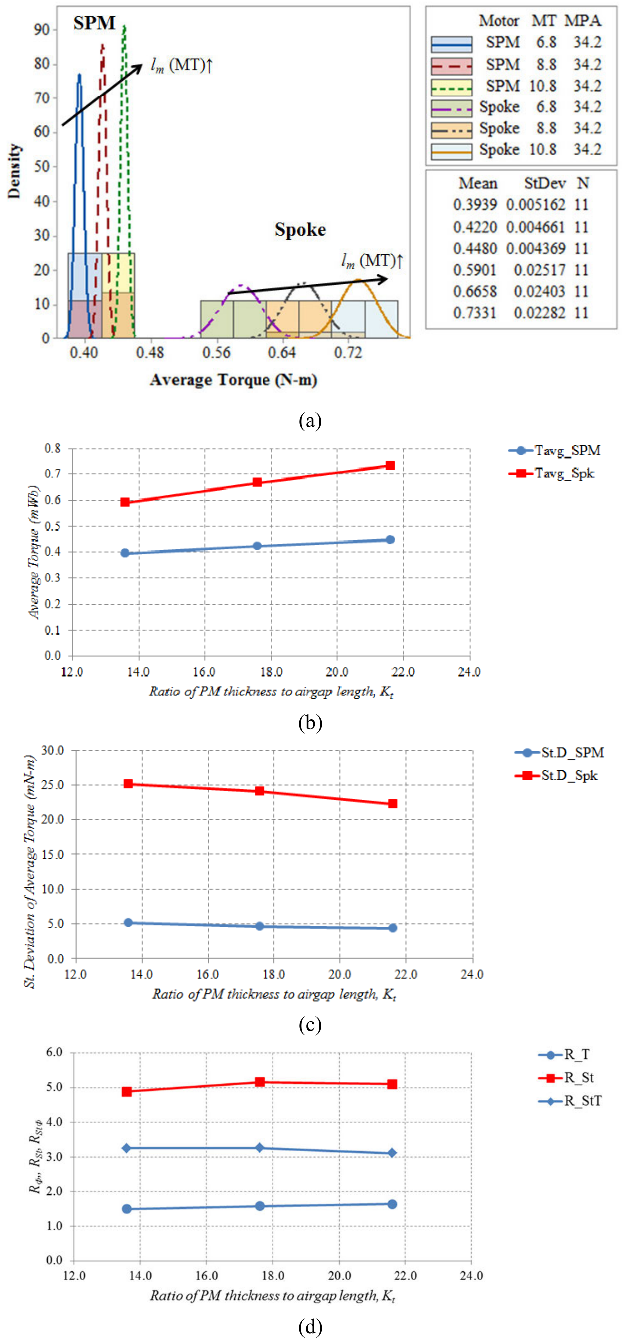

FIGURE 16. **Comparison of average torquesanalyzed by FEM between SPM and spoke-type PM machines inslotted statorbased on the PM thickness and the variations of the airgap length due to manufacturing tolerance (a)Probability distributions, (b) Mean values, (c) Standard deviations (d) Relative comparison indexes.**

PM thickness (MT) and the same rotor magnetic pole angle (MPA). As shown in the figure, the trend of each term is similar to that of the OCAF.

The overall trends agree well with those of the MEC results.

IV. CONCLUSION

The study focused on comparing the airgap flux density and its tolerance sensitivity caused by the variations in the airgap lengths including additional airgap lengths between spoke-type PM machine and SPM machine by using the MECs and their deduced equations. Subsequently, the results are verified via 2D-FEM.

The analysis and investigation results indicate that the spoke-type PM machines exhibit inherently higher sensitivity of the open-circuit airgap flux density and its mean value when compared to those of the SPM machines while assuming the same machine size.

Thus, it is very difficult to achieve both higher airgap flux density to increase torque/power density and its low sensitivity for a lower POF of the spoke-type PM machines.

A method to increase airgap flux density and decrease sensitivity involves adopting a thicker permanent magnet.

However, the method increases the material cost of the PM.

In conclusion, machine design engineers must perform the robust optimal design process between airgap flux density and its sensitivity and total solution design accounting for uncertainty, e.g., variations in the airgap length and PM dimensions due to manufacturing tolerances.

REFERENCES

[1] G. R. Slemon, "Electrical machines for variable-frequency drives," *Proc. IEEE*, vol. 82, no. 8, pp. 1123–1139, Aug. 1994.

[2] G. Pellegrino, A. Vagati, B. Boazzo, and P. Guglielmi, "Comparison of induction and PM synchronous motor drives for EV application including design examples," *IEEE Trans. Ind. Appl.*, vol. 48, no. 6, pp. 2322–2332, Nov./Dec. 2012.

[3] P. E. Kakosimos, A. G. Sarigiannidis, M. E. Beniakar, A. G. Kladas, and C. Gerada, "Induction motors versus permanent-magnet actuators for aerospace applications," *IEEE Trans. Ind. Electron.*, vol. 61, no. 8, pp. 4315–4325, Aug. 2014.

[4] T. R. Brinner, R. H. McCoy, and T. Kopecky, "Induction versus permanent-magnet motors for electric submersible pump field and laboratory comparisons," *IEEE Trans. Ind. Appl.*, vol. 50, no. 1, pp. 174–181, Jan. 2014.

[5] Z. Yang, F. Shang, I. P. Brown, and M. Krishnamurthy, "Comparative study of interior permanent magnet, induction, and switched reluctance motor drives for EV and HEV applications," *IEEE Trans. Transport. Electrific.*, vol. 1, no. 3, pp. 245–254, Oct. 2015.

[6] H.-J. Kim and J.-W. Moon, "Improved rotor structures for increasing flux per pole of permanent magnet synchronous motor," *IET Electr. Power Appl.*, vol. 12, no. 3, pp. 415–422, Mar. 2018.

[7] M. Onsal, B. Cumhur, Y. Demir, E. Yolacan, and M. Aydin, "Rotor design optimization of a new flux-assisted consequent pole spoke-type permanent magnet torque motor for low-speed applications," *IEEE Trans. Magn.*, vol. 54, no. 11, Nov. 2018, Art. no. 8206005.

[8] A. Fatemi, D. M. Ionel, M. Popescu, Y. C. Chong, and N. A. O. Demerdash, "Design optimization of a high torque density spoke-type PM motor for a formula E race drive cycle," *IEEE Trans. Ind. Appl.*, vol. 54, no. 5, pp. 4343–4354, Sep. 2018.

[9] E. Carraro, N. Bianchi, S. Zhang, and M. Koch, "Design and performance comparison of fractional slot concentrated winding spoke type synchronous motors with different slot-pole combinations," *IEEE Trans. Ind. Appl.*, vol. 54, no. 3, pp. 2276–2284, May/Jun. 2018.

[10] C.-S. Jun and B.-I. Kwon, "Performance comparison of a spoke-type PM motor with different permanent magnet shapes and the same magnet volume", *IET Electr. Power Appl.*, vol. 11, no. 7, pp. 1196–1204, Aug. 2017.

[11] X. Ge, Z. Q. Zhu, J. Li, and J. Chen, "A spoke-type IPM machine with novel alternate airspace barriers and reduction of unipolar leakage flux by step-staggered rotor," *IEEE Trans. Ind. Appl.*, vol. 52, no. 6, pp. 4789–4797, Nov./Dec. 2016.

[12] J. Li, K. Wang, and H. Zhang, "Flux-focusing permanent magnet machines with modular consequent-pole rotor," *IEEE Trans. Ind. Electron.*, to be published, doi: 10.1109/TIE.2019.2922922.

[13] A. M. El-Refaie, "Fractional-slot concentrated-windings synchronous permanent magnet machines: Opportunities and challenges," *IEEE Trans. Ind. Electron.*, vol. 57, no. 1, pp. 107–121, Jan. 2010.

[14] X. Sun, Z. Shi, G. Lei, Y. Guo, and J. Zhu, "Analysis, design and optimization of a permanent magnet synchronous motor for a campus patrol electric vehicle," *IEEE Trans. Veh. Technol.*, to be published, doi: 10.1109/TVT.2019.2939794.
[15] N. Baloch, J.-W. Kwon, M. Ayub, and B.-I. Kwon, "Low-cost dual-mechanical-port dual-excitation machine for washing machine application," *IEEE Access*, vol. 7, pp. 87141–87149, 2019.
[16] P. Lindh, I. Petrov, P. Immonen, J. Pyrhönen, M. Niemelä, J. Anttila, M. Paakkinen, and E. Scherman, "Performance of a direct-liquid-cooled motor in an electric bus under different load cycles," *IEEE Access*, vol. 7, pp. 86897–86905, 2019.
[17] C.-S. Jun and B.-I. Kwon, "Process capability control procedure for electrical machines by using a six-sigma process for achieving six-sigma quality level," *IET Electr. Power Appl.*, vol. 11, no. 8, pp. 1466–1474, Sep. 2017.
[18] C.-S. Jun, B.-I. Kwon, and O. Kwon, "Tolerance sensitivity analysis and robust optimal design method of a surface-mounted permanent magnet motor by using a hybrid response surface method considering manufacturing tolerances," *Energies*, vol. 15, no. 5, p. 1159, May 2018.
[19] Z. Q. Zhu, Z. Azar, and G. Ombach, "Influence of additional air gaps between stator segments on cogging torque of permanent-magnet machines having modular stators," *IEEE Trans. Magn.*, vol. 48, no. 6, pp. 2049–2055, Jun. 2012.
[20] H. Qian, H. Guo, Z. Wu, and X. Ding, "Analytical solution for cogging torque in surface-mounted permanent-magnet motors with magnet imperfections and rotor eccentricity," *IEEE Trans. Magn.*, vol. 50, no. 8, pp. 1–15, Aug. 2014.
[21] M. S. Islam, S. Mir, and T. Sebastian, "Issues in reducing the cogging torque of mass-produced permanent-magnet brushless DC motor," *IEEE Trans. Ind. Appl.*, vol. 40, no. 3, pp. 813–820, May/Jun. 2004.
[22] L. Gasparin, A. Cernigoj, S. Markic, and R. Fiser, "Additional cogging torque components in permanent-magnet motors due to manufacturing imperfections," *IEEE Trans. Magn.*, vol. 45, no. 3, pp. 1210–1213, Mar. 2009.
[23] G. Heins, T. Brown, and M. Thiele, "Statistical analysis of the effect of magnet placement on cogging torque in fractional pitch permanent magnet motors," *IEEE Trans. Magn.*, vol. 47, no. 8, pp. 2142–2148, Aug. 2011.
[24] J.-M. Kim, M.-H. Yoon, J.-P. Hong, and S.-I. Kim, "Analysis of cogging torque caused by manufacturing tolerances of surface-mounted permanent magnet synchronous motor for electric power steering," *IET Electr. Power Appl.*, vol. 10, no. 8, pp. 691–696, Sep. 2016.
[25] H. Guo, Z. Wu, H. Qian, K. Yu, and J. Xu, "Statistical analysis on the additional torque ripple caused by magnet tolerances in surface-mounted permanent magnet synchronous motors," *IET Electr. Power Appl.*, vol. 9, no. 3, pp. 183–192, Mar. 2015.
[26] A. J. P. Ortega and L. Xu, "Analytical prediction of torque ripple in surface-mounted permanent magnet motors due to manufacturing variations," *IEEE Trans. Ind. Appl.*, vol. 31, no. 4, pp. 1634–1644, Dec. 2016.
[27] N. Taran, V. Rallabandi, D. M. Ionel, P. Zhou, M. Thiele, and G. Heins, "A systematic study on the effects of dimensional and materials tolerances on permanent magnet synchronous machines based on the IEEE Std 1812," *IEEE Trans. Ind. Appl.*, vol. 55, no. 2, pp. 1360–1371, Mar./Apr. 2019.
[28] G. Bramerdorfer, "Tolerance analysis for electric machine design optimization: Classification, modeling and evaluation, and example," *IEEE Trans. Magn.*, vol. 55, no. 8, Aug. 2019, Art. no. 8106809.
[29] S. Lee, K. Kim, S. Cho, J. Jang, T. Lee, and J. Hong, "Optimal design of interior permanent magnet synchronous motor considering the manufacturing tolerances using Taguchi robust design," *IET Electr. Power Appl.*, vol. 8, no. 1, pp. 23–28, Jan. 2014.
[30] C. T. Krasopoulos, M. E. Beniakar, and A. G. Kladas, "Robust optimization of high-speed PM motor design," *IEEE Trans. Magn.*, vol. 53, no. 6, Jun. 2017, Art. no. 7207304.
[31] J.-G. Lee, N.-W. Hwang, H. R. Ryu, H.-K. Jung, and D.-K. Woo, "Robust optimization approach applied to permanent magnet synchronous motor," *IEEE Trans. Magn.*, vol. 53, no. 6, Jun. 2017, Art. no. 8001804.
[32] D. Hanselman, *Brushless Motors: Magnetic Design, Performance, and Control of Brushless DC and Permanent Magnet Synchronous Motors*. Orono, ME, USA: E-Man Press LLC, 2012, p. 24, 64–69, and 128–131.

CHA-SEUNG JUN was born in 1972. He received the B.S. and M.S. degrees in electrical engineering and the Ph.D. degree in electronic systems engineering from Hanyang University, Ansan, South Korea, in 1996, 1998, and 2018, respectively. From 1999 to 2000, he was a Research Engineer with the Delco Remy Korea, Ltd. Since 2000, he has been a Research Engineer and the Project Leader of the LG Electronics Inc., where he has performed lots of projects on the design and control of electric motors for home appliance. His current research interest includes the design and control of electric motors.

OHBONG KWON was born in 1970. He received the B.S. and M.S. degrees from the Department of Electrical Engineering, Hanyang University, Ansan, South Korea, in 1998 and 2000, respectively, and the Ph.D. degree from the Department of Electronic and Computer Engineering, University of Florida, Gainesville, FL, USA, in 2010. He has been an Assistant Professor with the Department of Computer Engineering Technology, New York City College of Technology, The City University of New York, since 2012. His current research interests include the design and control of electric motors, digital design, and control systems.

BYUNG-IL KWON was born in 1956. He received the B.S. and M.S. degrees in electrical engineering from Hanyang University, Ansan, South Korea, in 1981 and 1983, respectively, and the Ph.D. degree in electrical engineering and machine analysis from The University of Tokyo, Tokyo, Japan, in 1989. From 1989 to 2000, he was a Visiting Researcher with the Faculty of Science and Engineering Laboratory, University of Waseda, Tokyo, Japan. In 1990, he was a Researcher with the Toshiba System Laboratory, Yokohama, Japan. In 1991, he was a Senior Researcher with the Institute of Machinery and Materials Magnetic Train Business, Daejeon, South Korea. From 2001 to 2008, he was a Visiting Professor with the University of Wisconsin–Madison, Madison, WI, USA. He is currently a Professor with Hanyang University. His current research interest includes the design and control of electric machines.